Transfinite Mesh Update in Monolithic Fluid-Structure Simulations

F. Bérard[a], D. Couture-Peck[a], A. Garon[a], S. Étienne[a]

a. Polytechnique Montréal, Departement of mechanical engineering, felix.berard@polymtl.ca

Abstract

In r-adaptivity, several methods are available to extend boundary motion analytically into the computational domain. We propose a new mesh deformation technique based on transfinite mean value interpolation (TMI). In its original version TMI is explicit, matrix-free, and linearly exact, i.e., a solid rotation of the whole mesh is accurate. The mesh updating efficiency and robustness of the TMI, inverse distance weighting method (IDW) and radial basis functions method (RBF) are compared.

Résumé

Plusieurs méthodes sont présentement utilisées pour l'extension analytique du déplacement des noeuds de la frontière aux noeuds à l'intérieur du domaine. Nous proposons l'étude d'une nouvelle méthode d'interpolation nommée "Transfinite Mean value Interpolation" (TMI), qui possède deux principaux avantages sur certaines méthodes actuellement utilisées. Premièrement, elle est linéairement exacte, ainsi la rotation solide du maillage est calculée exactement sans dégradation du maillage initial. Ensuite, cette méthode est explicite et ne nécessite pas la résolution d'un système linéaire. Nous avons comparé cette nouvelle méthode à la méthode de distance inverse pondérée (IDW[1]) et à la méthode des bases radiales (RBF[1]), deux autres méthodes algébriques populaires.

Keyword : moving mesh methods, radial basis functions, inverse distance weighting method, mesh quality, transfinite mean value interpolation

1 Introduction

Fluid-structure interaction (FSI) problems are numerous in nature and engineering. For example the flow of blood in the arteries, the beating of the wing of the birds, and the rolling motion of the Wright Brothers Flyer obtained through wing-warping. In fluid mechanics, the Arbitrary Lagrangian-Eulerian (ALE)[4] formulation of the Navier-Stokes equations is unquestionably the most used to describe these problems. The Navier-Stokes equations and the elasticity equations are solved together to predict the forces on the solid and the dynamic of the flow. The domain of application often dictates the level of interoperability between the different solvers involved in the simulation. For example, modelling the interaction between a submerged buoy and the flow of water requires monolithic calculation [4] [5] of

[1] acronyme anglais

the fluid's degrees of freedom, the solid's distortions, and the displacements of the mesh's nodes to ensure the calculations stability and convergence. Another similar application involves modelling the interaction of submerged pipelines [9] from the well to the offshore platform. The usual weakly coupled approach, in which the fluid's degrees of freedom and the structure are solved sequentially, can not solve this type of problem [15]. All ALE formulations have either an algebraic or a partial differential set of equations to update the mesh to the motion of the solid. In these formulations, the convective acceleration of the flow is a function of the fluid and the mesh velocities. While the pseudo-solid method is certainly the most prevalent and has been successfully applied to monolithic and weakly coupled simulations of fluid-structure interaction problems, algebraic methods are easier to implement and are widely used in aeroelasticity or when the fluid-structure interaction problem can be solved sequentially.

1.1 Contribution of this study

The object of this paper is the study and characterization of mesh adaptation (r-adaptivity) with transfinite mean value interpolation (TMI). In mesh updating, the TMI method is new and possesses intrinsic properties which, at first glance, make it interesting for FSI simulations, i.e. it is linearly exact and matrix-free. Therefore, it is our goal to reveal its strengths and weaknesses for FSI mesh-updating through direct comparison with the inverse distance weighting method (IDW) and radial basis functions (RBF) method.

2 Methods

In this section, we briefly recall the mathematics of the interpolation methods used in mesh-updating. For a detailed description of TMI, RBF and IDW, we refer the reader to Garon and Delfour [6], Rendall and Allen [10] and Witteveen and Bilj [14], respectively.

2.1 TMI

The TMI method of Dyken and Floater [3] interpolates a function $f(\xi)$, defined on $\partial\Omega$ of Ω at every point $\mathbf{x} \in \Omega \setminus \partial\Omega$. We name $u(\mathbf{x})$ the result of the interpolation in

$$u(\mathbf{x}) = \frac{\displaystyle\int_{\partial\Omega} \frac{f(\xi)(\xi - \mathbf{x}) \cdot \mathbf{n} d\Gamma}{||\mathbf{x} - \xi||^k}}{\displaystyle\int_{\partial\Omega} \frac{(\xi - \mathbf{x}) \cdot \mathbf{n} d\Gamma}{||\mathbf{x} - \xi||^k}} \tag{1}$$

where $\xi \in \partial\Omega$. In this relationship, the parameter k controls the behaviour of the interpolation in the neighbourhood of $\partial\Omega$, When $k = n + 1$, with n the space dimension, the TMI method is linearly accurate.

2.2 RBF

RBF or kriging uses radial basis function to interpolate a function known on a discrete finite number of nodes $E = \{\xi_1, \xi_2, ..., \xi_m\}$, that is to say the values of $f(\xi_i)$. In this method, the solution of the linear system :

$$\begin{bmatrix} \varphi(||\xi_\mathbf{1} - \xi_\mathbf{1}||) & ... & \varphi(||\xi_\mathbf{1} - \xi_\mathbf{m}||) \\ ... & ... & ... \\ \varphi(||\xi_\mathbf{m} - \xi_\mathbf{1}||) & ... & \varphi(||\xi_\mathbf{m} - \xi_\mathbf{m}||) \end{bmatrix}_{m \times m} \begin{bmatrix} \lambda_1 \\ ... \\ \lambda_m \end{bmatrix} = \begin{bmatrix} f(\xi_\mathbf{1}) \\ ... \\ f(\xi_\mathbf{m}) \end{bmatrix} \tag{2}$$

yields the interpolation method coefficients $\{\lambda_1, ...\lambda_n\}$ of $u(\mathbf{x})$

$$u(\mathbf{x}) = \sum_{j=1}^{m} \lambda_j \varphi(||\mathbf{x} - \xi_\mathbf{j}||) \tag{3}$$

Among the functions proposed by Wendland [12], we study five, which according to De Boer et al. [2] are the most suitable for mesh-updating. Note that we have deliberately omitted the linear constraint on the solution to the interpolation coefficients as it is one of the current instantiations.

2.3 IDW

The IDW method of Shepard [11] interpolates a function known on a discrete finite number of nodes $E = \{\xi_1, \xi_2, ..., \xi_m\}$, that is to say the values of $f(\xi_i)$. We name $u(\mathbf{x})$ the result of the interpolation in

$$u(x) = \frac{\displaystyle\sum_{j=1}^{m} \frac{f(\xi_\mathbf{j})}{||\mathbf{x} - \xi_\mathbf{j}||^k}}{\displaystyle\sum_{j=1}^{m} \frac{1}{||\mathbf{x} - \xi_\mathbf{j}||^k}} \tag{4}$$

where $\xi \in \partial\Omega$. The parameter k controls the behaviour of the interpolation in the neighbourhood of E.

2.4 Mesh quality

To measure the efficiency of interpolation methods in mesh-updating, we use the mesh quality metric proposed by Knupp [8] and previously used by De Boer et al. [2] :

$$f_{ss} = f_{shape} \times f_{size} \tag{5}$$

where f_{size} measures the surface ratio of an element between the deformed and underformed state; $f_{size} = 0$ when the element is either entangled or degenerated, and $f_{size} = 1$ when the surface is conserved. f_{shape} measures how close the element is to an equilateral triangle; $f_{shape} = 0$ when the element is degenerated, and $f_{size} = 1$ when the element is a perfect equilateral triangle. However, to compare the TMI, IDW and RBF methods on an equal basis, it is preferable to normalize the quality measurements by their respective asymptotic value. We measure $(f_{ss})_\infty$ by updating the vertices with a large numbers of steps, and then compute each step with a high order integration method, namely 4th order Runge-Kutta (RK4). Thus, we define :

$$\min(f_{ss})_{rel} = \frac{\min(f_{ss})}{\min(f_{ss})_\infty} \tag{6}$$

2.5 Mesh-updating

To integrate the mesh vertices along their path from the undeformed state to the deformed state, we study the cost and efficiency of Euler and RK4 methods. We use the metric defined by Equation (6) to measure the quality of the updated meshes.

We validated the results with three meshes with an increasing number of vertices. The results for TMI, IDW and RBF methods with regards to the integration method are globally independent of the mesh

density. Figure 1b is an example of the coarser mesh used in this study, while Table 1a shows the behavior of the RBF mesh-updating with CPC2 and TPS functions (see Table 2).

For a known integration method, the computational cost is proportional to the number of calls to the interpolation method, i.e., the workload. For example, for a workload of eight, we call the Euler integration method eight times per step and the RK4 twice per step. At equal workload, the computation times of Euler and RK4 integration methods are almost identical as shown in Table 1b. Of course, a finer mesh requires more computational time, but at equal workload it is approximatively the same for Euler and RK4 methods. As one can see in Table 1a, the asymptotic value is reached at a faster rate with the RK4 integration than with Euler integration. Henceforth, we will use only RK4 integration for the numerical tests.

Table 1: Relative mesh quality for Test case 1 using RBF method and the coarser mesh.

(a) Relative mesh quality depending on the workload

	Euler		RK4	
Workload	CPC2	TPS	CPC2	TPS
1	0.000	0.000	-	-
2	0.228	0.266	-	-
4	0.683	0.698	0.724	0.776
8	0.854	0.863	0.945	0.959
12	0.904	0.910	0.976	0.982
16	0.929	0.933	0.987	0.990
32	0.965	0.967	0.997	0.998
64	0.983	0.984	**0.999**	**0.999**
128	0.991	0.992	1.000	1.000
256	0.996	0.996	1.000	1.000
512	**0.998**	**0.998**	1.000	1.000

(b) Time [sec] to compute each test from table 1a

	Euler		RK4	
Workload	CPC2	TPS	CPC2	TPS
1	< 1	< 1	-	-
2	< 1	< 1	-	-
4	< 1	< 1	< 1	< 1
8	< 1	< 1	< 1	< 1
12	< 1	< 1	< 1	< 1
16	< 1	< 1	< 1	< 1
32	1	< 1	1	< 1
64	2	1	2	1
128	3	2	3	2
256	7	3	7	3
512	13	7	14	7

3 Numerical tests

3.1 Test case 1: A rotating ellipse

In this first test, we study mesh-updating of an ellipse rotated 120 degrees anti-clockwise about its center. The following equations give the solid rotation of the mesh vertices on the ellipse:

$$x_{new} = x\cos(\theta) - y\sin(\theta)$$
$$y_{new} = y\cos(\theta) + x\sin(\theta)$$

We selected this test case because of its relevance to some large deformations FSI problems (see Weymouth [13]). Also, the geometry of this test is sufficiently smooth to allow the vertices to move freely on its boundary. We investigate this type of motion in section 3.3. Figure 1a illustrates the general geometry of the test, while Figures 1b, 1c and 1d illustrate the meshes used for the tests.

Results

As mentioned in section 2, a parameter value k or a weighting function modify the behavior of the interpolation method. Tables 3, 4 and 5 show the results with three values of the exponent k of the

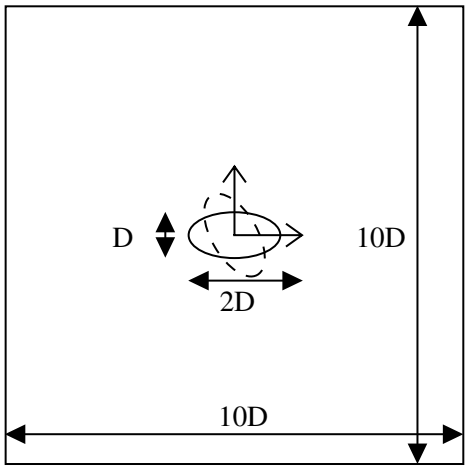

(a) General description.

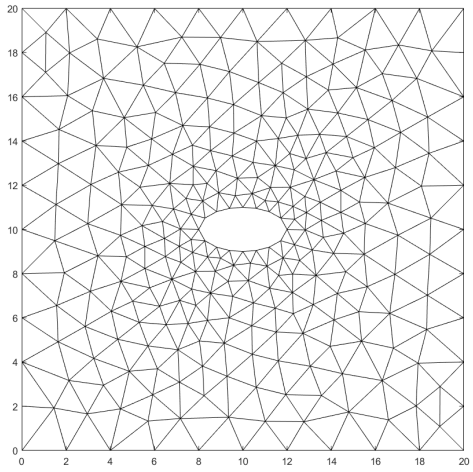

(b) Initial Mesh - Coarse - 284 nodes.

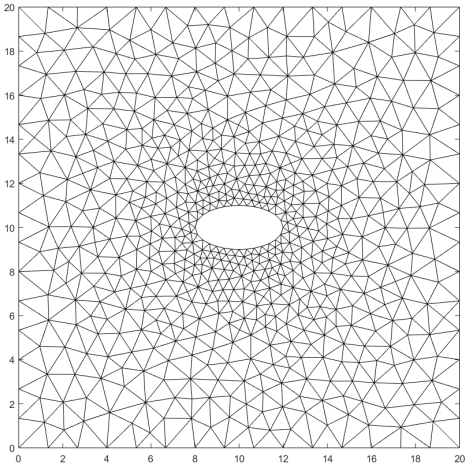

(c) Initial Mesh - Normal - 678 nodes.

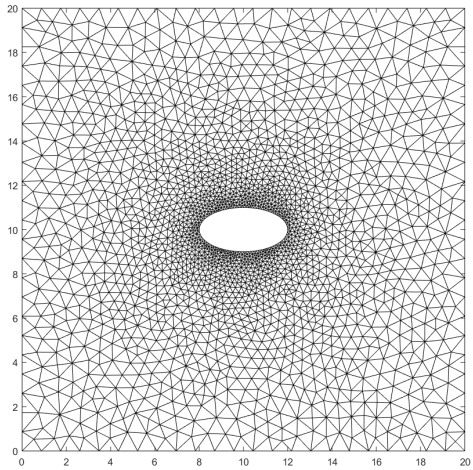

(d) Initial Mesh - Fine - 2240 nodes.

Figure 1: Description and initial meshes of Test Case 1.

distance function involved in the computation of the TMI and IDW methods. These tables also include the results of three of the five RBF radial functions. For comparison purposes only, bold values indicate when the normalized quality is within the interval [0.998,1.002]. Also, 0.000 means that the mesh contains at least one entangled element. Both TMI and IDW produce invalid meshes for the coarser and normal mesh. Figure 2a shows an IDW updated mesh where entangled elements are localized along the ellipse boundary. These tests indicate that $k = 4$ and $k = 5$ are the optimal parameter value for the TMI and IDW methods, respectively. However, all RBF radial functions yield good quality meshes at a lower cost than TMI and IDW methods.

Figures 2b, 2c and 2d show examples of updated meshes. The coarser mesh was chosen to illustrate the behavior of each interpolation method. We observe that the IDW and TMI methods update the nodes in a neighborhood surrounding the moving boundary; an increase of the value of the exponent increases the size of the region of influence. Figures 4b, 4c and 4d show that this gain is marginal for values greater than or equal to $k = 5$. On the other hand, RBF mesh updating moves vertices farther and distributes them more evenly. All RBF functions yields similar meshes.

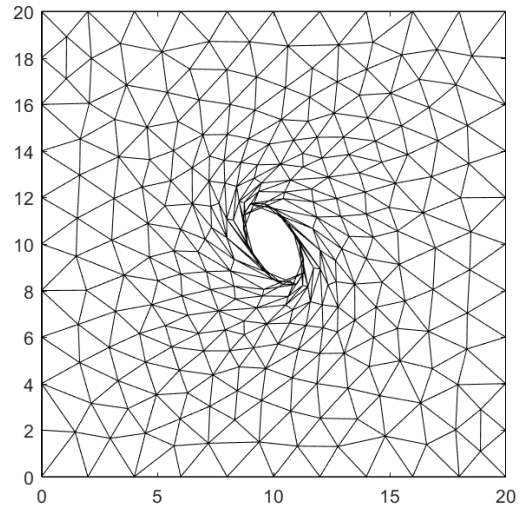

(a) Example of degenerated mesh.

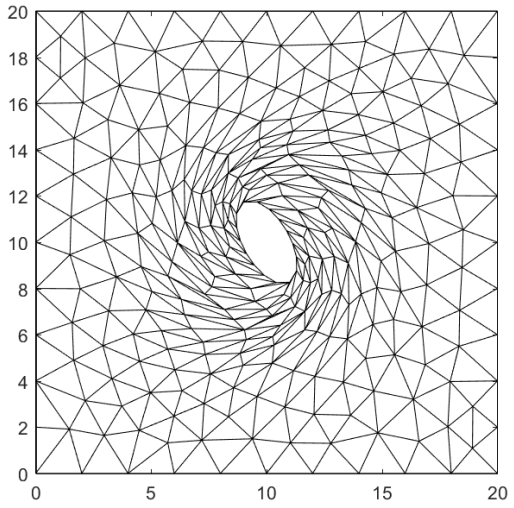

(b) Final mesh.

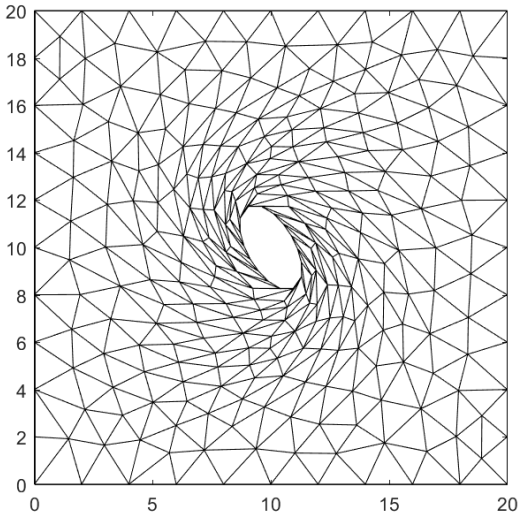

(c) Final mesh.

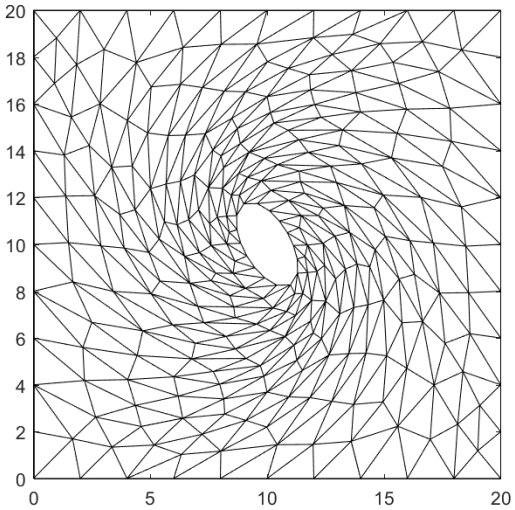

(d) Final mesh.

Identifier	Mesh	Method	Parameter	Workload
(a)	Coarse	IDW	$k = 3$	4
(b)	Coarse	TMI	$k = 4$	256
(c)	Coarse	IDW	$k = 4$	256
(d)	Coarse	RBF	TPS	256

Figure 2: Final meshes for multiple subtests of Test case 1.

3.2 Test case 2: Channel flow with a wall-mounted flexible body

Another classical FSI benchmark problem is the simulation of a flexible beam in a channel. We used the geometry inspired from Fortin et al. [7] illustrated in Figure 3a. However, we used the kinematic proposed by Barral [1] and described by Equations (7) and (8):

$$x_{new} = x(0) + (R - x(0))(1 - \cos(\theta)) \quad (7)$$

$$y_{new} = (R - x(0))\sin(\theta) \quad (8)$$

Table 2: List of radial basis functions investigated.

	Name	Formula
1	CPC2	$(1-x)^4(4x+1)$
2	CTPSC1	$1+(80/3)x^2-40x^3+15x^4-(8/3)x^5+20x^2\ln(x)$
3	CTPSC2A	$1-30x^2-10x^3+45x^4-6x^5-60x^3\ln(x)$
4	CTPSC2B	$1-20x^2+80x^3-45x^4-16x^5+60x^4\ln(x)$
5	TPS	$x^2\ln(x)$

Table 3: Relative mesh quality from Test case 1 for the coarser mesh.

	TMI			IDW			RBF		
Workload	3	4	5	3	4	5	CPC2	CTPSC1	TPS
4	*0.000*	*0.000*	*0.000*	*0.000*	*0.000*	*0.000*	0.259	0.724	0.776
16	*0.000*	0.840	*0.000*	*0.000*	*0.000*	*0.000*	1.012	0.987	0.990
64	*0.000*	0.990	*0.000*	*0.000*	*0.000*	*0.000*	**1.001**	**0.999**	**0.999**
256	*0.000*	**1.000**	*0.000*	*0.000*	*0.000*	*0.000*	1.000	1.000	1.000
512	*0.000*	1.000	*0.000*	*0.000*	*0.000*	*0.000*	1.000	1.000	1.000

Table 4: Relative mesh quality from Test case 1 for the normal mesh.

	TMI			IDW			RBF		
Workload	3	4	5	3	4	5	CPC2	CTPSC1	TPS
4	*0.000*	0.049	*0.000*	*0.000*	*0.000*	*0.000*	0.713	0.862	0.909
16	*0.000*	0.837	0.547	*0.000*	*0.000*	0.008	0.997	**1.000**	1.002
64	*0.000*	0.990	0.969	*0.000*	*0.000*	0.893	**1.000**	1.000	**1.000**
256	*0.000*	**1.000**	**0.998**	*0.000*	*0.000*	0.995	1.000	1.000	1.000
512	*0.000*	1.000	1.000	*0.000*	*0.000*	**1.000**	1.000	1.000	1.000

Table 5: Relative mesh quality from Test case 1 for the finer mesh.

	TMI			IDW			RBF		
Workload	3	4	5	3	4	5	CPC2	CTPSC1	TPS
4	*0.000*	0.310	*0.000*	*0.000*	*0.000*	*0.000*	0.564	1.056	1.028
16	0.949	0.976	0.967	0.646	0.933	0.946	0.987	**1.000**	**1.002**
64	0.991	**0.999**	0.998	0.977	0.996	0.997	**1.000**	1.000	1.000
256	**1.000**	1.000	**1.000**	**0.999**	**1.000**	**1.000**	1.000	1.000	1.000
512	1.000	1.000	1.000	1.000	1.000	1.000	1.000	1.000	1.000

with

$$\theta = \frac{x(0)}{R}, \quad R = R_{min} + (R_{max} - R_{min})\frac{e^{-\kappa\mu} - e^{-\kappa}}{1 - e^{-\kappa}}$$

where μ is a shape parameter, that is $\mu = 0$ corresponds to the initial state and $\mu = 1$ corresponds to the final state. The parameters for this problem are $\kappa = 10$, $R_{min} = 3$, $R_{max} = 400$. The results are given in Tables 6, 7 and 8.

Results

In this test case, we observed fewer entangled elements than with test Case 1. Mesh-updating performed well with the three interpolation methods except for the TMI and the IDW methods for $k = 3$, where we observed entangled elements in the vicinity of the flexible beam (see Figure 4a). For the TMI method,

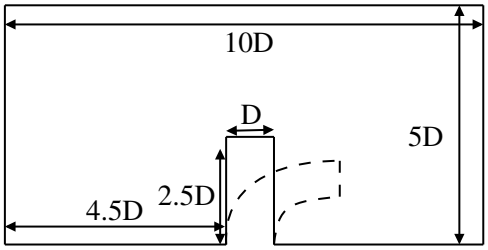

(a) General description of the second Test Case 2.

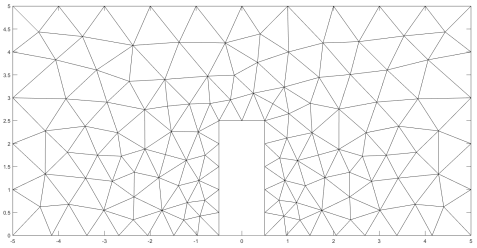

(b) Initial Mesh - Coarse - 141 nodes.

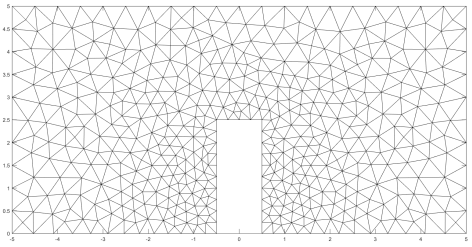

(c) Initial Mesh - Normal - 483 nodes.

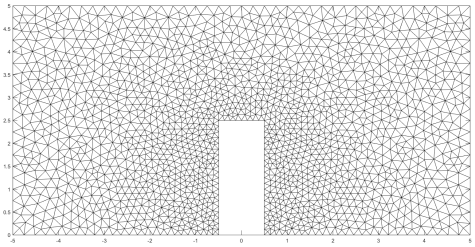

(d) Initial Mesh - Fine - 1802 nodes.

Figure 3: Description and initial meshes of Test Case 2.

Figures 4a, 4b and 4c show the influence of the parameter k on the concentration of vertices near the beam. An increase in the value of the parameter moves this region farther.

The IDW method produces fewer invalid meshes than for the previous test, with only one exponent value producing invalid meshes – see Figure 4d for an example of a valid mesh. Once again, all RBF functions yield good quality meshes and Figures 4e and 4f show the final updated mesh for the CPC2 and TPS radial functions.

The convergence rate for this test case is better than for test case 1 for the IDW and RBF methods, but not for TMI method which requires a significant number of steps.

3.3 Test case 3: A rotating ellipse (by deformation)

In this test case, we replace the rotating motion by an equivalent deformation that allows the boundary vertices to move freely on the ellipse boundary. This technique allows complete rotation without significant mesh distortion. We propose a new way to simulate solid rotation. The object is instead deformed from initial to final state. The motion is now given by the following equations:

$$\begin{aligned} \hat{\theta} &= \tan^{-1}\left(\frac{a}{b}\tan(\bar{\theta}-\beta)\right) \\ r &= \sqrt{a^2\cos(\hat{\theta}) + b^2\sin(\hat{\theta})} \\ x_{new} &= r\cos(\bar{\theta}) \\ y_{new} &= r\sin(\bar{\theta}) \end{aligned}$$

with a the minor axis of the ellipse, b the major axis, $\bar{\theta} = \tan(\frac{x}{y})$ and β the rotation angle. The results are presented in Tables 9, 10 and 11.

Results

In this last test, we replaced solid rotation with an equivalent deformation. This transformation reduces the nodes motion considerably and therefore minimizes the computational workload. The interpolation-

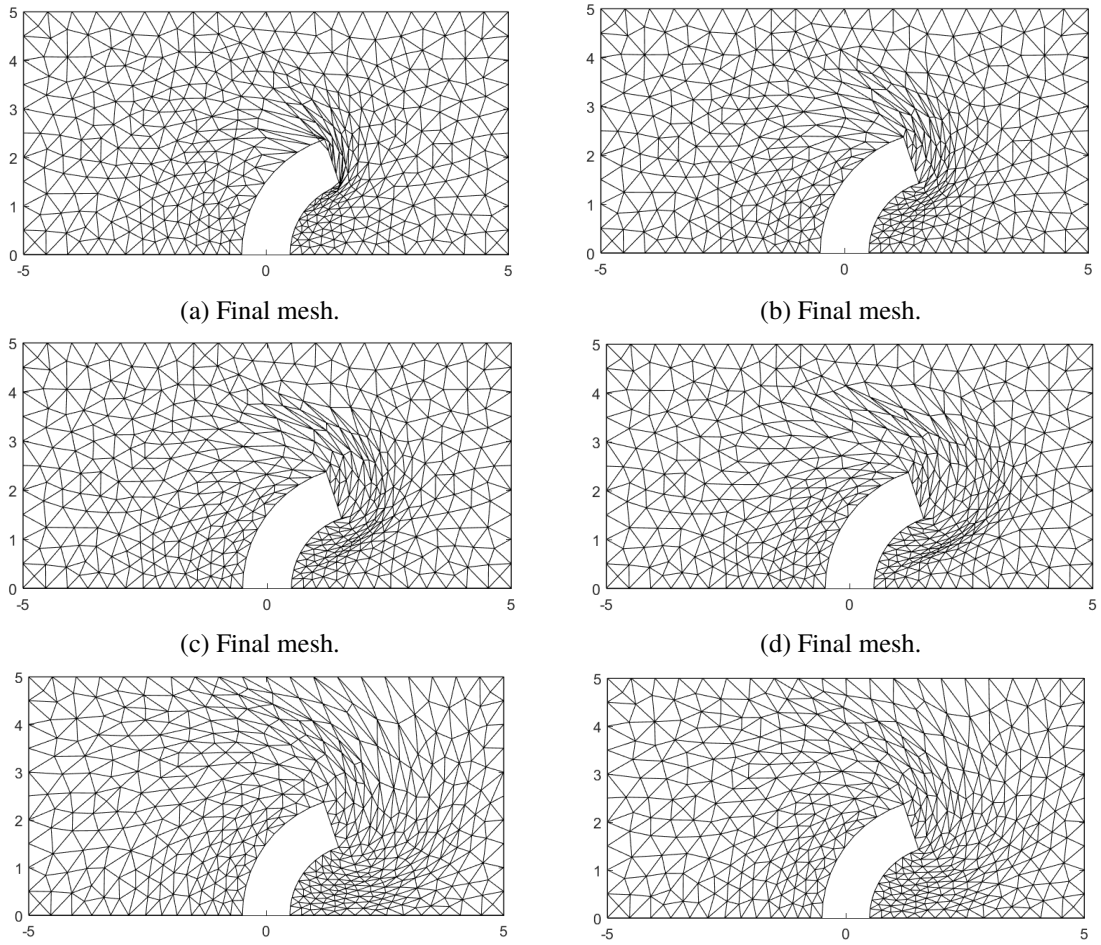

(a) Final mesh. (b) Final mesh.

(c) Final mesh. (d) Final mesh.

(e) Final mesh. (f) Final mesh.

Identifier	Mesh	Method	Parameter	Workload
(a)	Normal	TMI	$k = 3$	256
(b)	Normal	TMI	$k = 4$	256
(c)	Normal	TMI	$k = 5$	256
(d)	Normal	IDW	$k = 5$	256
(e)	Normal	RBF	CPC2	256
(f)	Normal	RBF	TPS	256

Figure 4: Final meshes for multiple subtest of test case 2.

based r-adaptivity performed well except for the RBF method for compact radial bases CPC2 and CTPSC1. This result is unexpected and needs to be confirmed.

With this shape transformation, the vertices move freely on the ellipse. However, this motion is only apparent since the methodology interpolates the vertices coordinates linearly between the initial position and the final position. This transformation makes it possible to better preserve the characteristics of the initial mesh, such as the shape and size of the elements. Figures 5b, 5c and 5d show the final updated meshes, for the TMI, IDW and RBF methods, among which we found no significant differences.

4 Conclusion

We investigated and characterized interpolation-based mesh updating with transfinite mean value interpolation (TMI), inverse distance weighting (IDW) and radial basis functions (RBF).

Table 6: Relative mesh quality from Test case 2 for the coarser mesh.

	TMI			IDW			RBF		
Workload	3	4	5	3	4	5	CPC2	CTPSC1	TPS
4	*0.000*	0.463	1.167	0.442	1.182	1.316	1.017	0.954	0.945
16	*0.000*	0.953	1.021	0.907	1.026	1.068	**1.001**	0.994	0.993
64	*0.000*	0.996	**1.001**	0.992	**1.002**	1.003	1.000	**1.000**	**1.000**
256	*0.000*	**1.000**	1.000	**1.000**	1.000	**1.000**	1.000	1.000	1.000
512	*0.000*	1.000	1.000	1.000	1.000	1.000	1.000	1.000	1.000

Table 7: Relative mesh quality from Test case 2 for the normal mesh.

	TMI			IDW			RBF		
Workload	3	4	5	3	4	5	CPC2	CTPSC1	TPS
4	*0.000*	*0.000*	0.085	*0.000*	0.375	1.015	0.835	1.046	1.050
16	*0.000*	0.224	0.802	*0.000*	0.899	1.032	0.975	1.008	1.010
64	*0.000*	0.920	0.984	*0.000*	0.992	**1.001**	**0.998**	**1.001**	**1.001**
256	*0.000*	0.996	**0.999**	*0.000*	**1.000**	1.000	1.000	1.000	1.000
512	*0.000*	**1.000**	1.000	*0.000*	1.000	1.000	1.000	1.000	1.000

Table 8: Relative mesh quality from Test case 2 for the finer mesh.

	TMI			IDW			RBF		
Workload	3	4	5	3	4	5	CPC2	CTPSC1	TPS
4	*0.000*	0.742	0.889	0.603	0.910	1.247	0.894	**1.000**	1.006
16	*0.000*	0.954	0.975	0.908	0.986	1.041	0.984	1.001	1.002
64	*0.000*	0.996	0.998	0.992	**0.999**	1.002	**0.999**	1.000	**1.000**
256	*0.000*	**1.000**	**1.000**	**1.000**	1.000	**1.000**	1.000	1.000	1.000
512	*0.000*	1.000	1.000	1.000	1.000	1.000	1.000	1.000	1.000

1. In the first test case RBF outperformed the two algebraic methods in robustness and rate of convergence. On the other hand, the TMI and IDW methods yielded good quality meshes for the finest mesh (Figure 1d) with optimal exponent $k = 4$ and $k = 5$, respectively.

2. In the second test case, RBF outperformed the TMI and IDW methods. Nevertheless, the TMI and IDW methods yielded good quality meshes for the coarser, normal, and finest meshes with optimal exponent $k = 5$ and $k = 5$, respectively (Figures 3c-3d).

3. In the third test case, we allowed the vertices to move freely on the boundary of an ellipse under rotation. The TMI and the IDW were more robust than the RBF mesh-updating with parameters values between 3 and 5, inclusively, yielding similar rates of convergence. However, compact support radial functions yielded entangled meshes.

Acknowledgements

Financial support from the Simulation-based Engineering Science (Génie Par la Simulation) program funded through the CREATE program from the Natural Sciences and Engineering Research Council of Canada is gratefully acknowledged.

Table 9: Relative mesh quality from Test case 3 for the coarser mesh.

	TMI			IDW			RBF		
Workload	3	4	5	3	4	5	CPC2	CTPSC1	TPS
4	**1.000**	**1.001**	1.003	**1.001**	1.003	1.004	*0.000*	*0.000*	0.994
16	1.000	1.000	**1.000**	1.000	**1.000**	**1.000**	*0.000*	*0.000*	**1.000**
64	1.000	1.000	1.000	1.000	1.000	1.000	*0.000*	*0.000*	1.000
256	1.000	1.000	1.000	1.000	1.000	1.000	*0.000*	*0.000*	1.000
512	1.000	1.000	1.000	1.000	1.000	1.000	*0.000*	*0.000*	1.000

Table 10: Relative mesh quality from Test case 1 for the normal mesh.

	TMI			IDW			RBF		
Workload	3	4	5	3	4	5	CPC2	CTPSC1	TPS
4	0.997	0.992	0.988	1.003	**0.999**	0.991	*0.000*	*0.000*	0.986
16	**1.000**	**1.000**	**1.000**	**1.000**	1.000	**1.000**	*0.000*	*0.000*	**1.000**
64	1.000	1.000	1.000	1.000	1.000	1.000	*0.000*	*0.000*	1.000
256	1.000	1.000	1.000	1.000	1.000	1.000	*0.000*	*0.000*	1.000
512	1.000	1.000	1.000	1.000	1.000	1.000	*0.000*	*0.000*	1.000

Table 11: Relative mesh quality from Test case 1 for the finer mesh.

	TMI			IDW			RBF		
Workload	3	4	5	3	4	5	CPC2	CTPSC1	TPS
4	**0.999**	0.982	0.976	0.977	0.990	**1.000**	*0.000*	*0.000*	0.997
16	1.000	**1.000**	**1.000**	**1.000**	**1.000**	1.000	*0.000*	*0.000*	**1.000**
64	1.000	1.000	1.000	1.000	1.000	1.000	*0.000*	*0.000*	1.000
256	1.000	1.000	1.000	1.000	1.000	1.000	*0.000*	*0.000*	1.000
512	1.000	1.000	1.000	1.000	1.000	1.000	*0.000*	*0.000*	1.000

References

[1] Nicolas Barral, Edward Luke, and Frédéric Alauzet. Two Mesh Deformation Methods Coupled with a Changing-connectivity Moving Mesh Method for CFD Applications.

[2] A. de Boer, M.S. van der Schoot, and H. Bijl. Mesh deformation based on radial basis function interpolation. *Computers & Structures*, 85(11):784–795, 2007.

[3] Christopher Dyken and Michael S. Floater. Transfinite mean value interpolation. *Computer Aided Geometric Design*, 26(1):117–134, 2009.

[4] Stephane Etienne, Dominique Pelletier, and Andre Garon. A Monolithic Formulation for Steady-State Fluid-Structure Interaction Problems. In *34th AIAA Fluid Dynamics Conference and Exhibit*, Portland, Oregon, June 2004. American Institute of Aeronautics and Astronautics.

[5] Miguel A. Fernández and Jean-Frédéric Gerbeau. Algorithms for fluid-structure interaction problems. In Luca Formaggia, Alfio Quarteroni, and Alessandro Veneziani, editors, *Cardiovascular Mathematics*, pages 307–346. Springer Milan, Milano, 2009.

[6] A. Garon and M. Delfour. Mesh adaptation based on transfinite mean value interpolation. *in press*, 2019.

[7] A. Jendoubi, J. Deteix, and A. Fortin. A simple mesh-update procedure for fluid–structure interaction problems. *Computers & Structures*, 169:13–23, June 2016.

[8] Patrick M. Knupp. Algebraic mesh quality metrics for unstructured initial meshes. *Finite Elements in Analysis and Design*, 39(3):217–241, January 2003.

[9] Juan P. Pontaza and Raghu G. Menon. Prediction of Vortex-Induced Vibration Response of a Pipeline Span by Coupling a Viscous Flow Solver and a Beam Finite Element Solver. *Journal of Offshore Mechanics and Arctic Engineering*, 135(3):031702, May 2013.

[10] T. C. S. Rendall and C. B. Allen. Unified fluid–structure interpolation and mesh motion using radial basis functions. *International Journal for Numerical Methods in Engineering*, 74(10):1519–1559, June 2008.

[11] Donald Shepard. A Two-dimensional Interpolation Function for Irregularly-spaced Data. In *Proceedings of the 1968 23rd ACM National Conference*, ACM '68, pages 517–524. ACM, 1968.

[12] Holger Wendland. *Konstruktion und Untersuchung radialer Basisfunktionen mit kompaktem Träger*. PhD thesis, Dissertation der Georg-August-Universität zu Göttingen, Georg-August-Universität Göttingen, Wilhelmsplatz 1 (Aula), 37073 Göttingen, 1996.

[13] G. D. Weymouth. Chaotic rotation of a towed elliptical cylinder. *Journal of Fluid Mechanics*, 743:385–398, March 2014.

[14] Jeroen Witteveen and Hester Bijl. Explicit Mesh Deformation Using Inverse Distance Weighting Interpolation. In *19th AIAA Computational Fluid Dynamics*. American Institute of Aeronautics and Astronautics, December 2018.

[15] Stéphane Étienne and Dominique Pelletier. The low Reynolds number limit of vortex-induced vibrations. *Journal of Fluids and Structures*, 31:18–29, 2012.

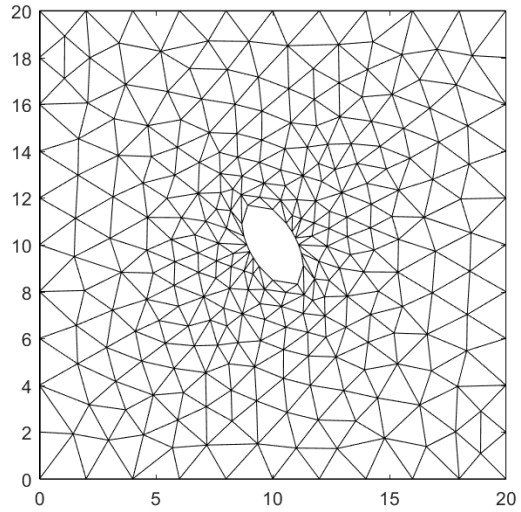

(a) Final mesh.

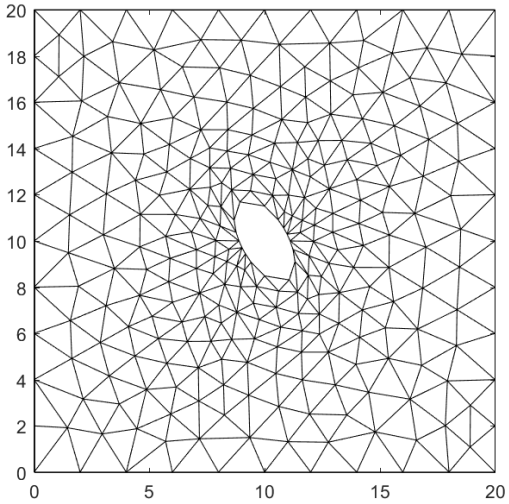

(b) Final mesh.

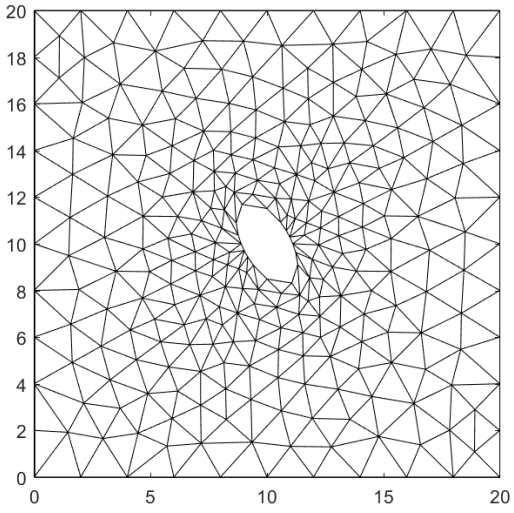

(c) Final mesh.

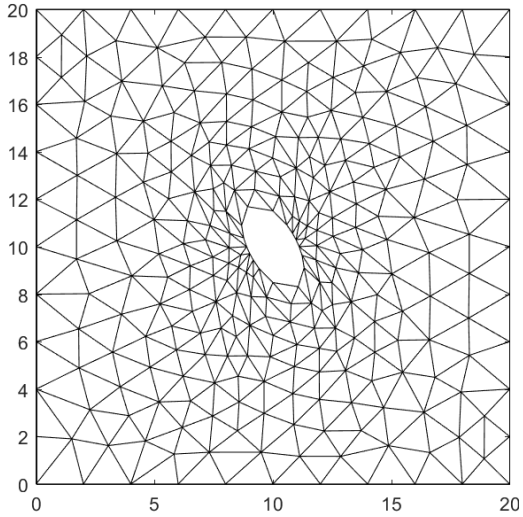

(d) Final mesh.

Identifier	Mesh	Method	Parameter	Workload
(a)	Coarse	IDW	$k = 3$	4
(b)	Coarse	TMI	$k = 4$	256
(c)	Coarse	IDW	$k = 4$	256
(d)	Coarse	RBF	TPS	256

Figure 5: Final meshes for multiple subtest of test case 3.